Effective Polarization-Based Image Dehazing With Regularization Constraint

Zheng Liang, Xueyan Ding, Zetian Mi, Yafei Wang, and Xianping Fu

***Abstract*— Image taken in turbid media generally exists poor visibility and low contrast, which results from attenuation of the propagated light. In this letter, an effective polarization-based image dehazing method is proposed, which relies on the relationship between the angle of polarization (AoP) from the Stokes vector and the scattered light. To avoid the influence of noise, AoP is optimized based on regularization constraints. The regularization function is made using an assumption that adjacent pixels with similar colors have similar values of AoP. Moreover, according to the revised AoP information, all the key parameters can be effectively and automatically estimated without considering the no-object region (or the sky region) exists or not, which relies on a frequency prior strategy. Extensive experiments on real-world images demonstrate that the proposed method is more effective than several previous image restoration or enhancement works.**

***Index Terms*— Angle of polarization (AoP), polarization-based dehazing, scattering media, stokes vector.**

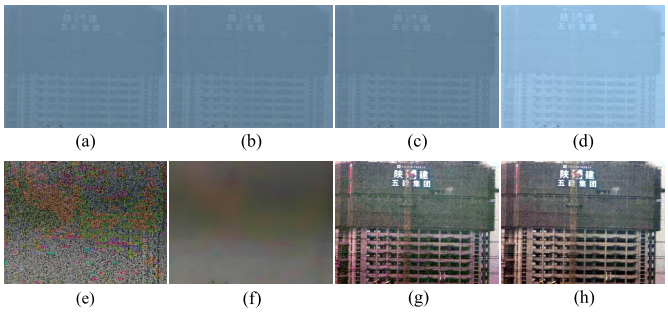

Fig. 1. Dehazed result generated by the proposed method. (a)–(c) Polarimetric images captured under the specific angle of the polarizer 0°, 45°, and 90°, respectively. (d) Total intensity image. (e) and (f) Initial and optimized AoP image, respectively. (g) and (h) Restored image yielded using the initial AoP image and optimized AoP image, respectively.

I. Introduction

ACQUISITION of clear image is an important subject for many scientific remote sensing missions, such as remote control of underwater robot [1], marine biology, and ecological research [2]–[4]. However, images captured in turbid media (fog, haze, and water) generally suffer from strong wavelength-dependent absorption and scattering. The scattering effect redirects light propagation into other directions and makes unwanted scattered light into the optical camera, leading to low contrast and generating a haze that superimposes itself on the image. The absorption effect reduces the energies of ambient light according to different wavelengths, which makes the image visually generating color distortion such as greenish and bluish. Thus, an effective method to enhance the visibility of such degraded image is valuable for numerous applications.

The techniques used to enhance the visibility of degraded image can be roughly grouped in two classes: methods based on single image [5]–[7] and methods that employ multiple images [8]–[10]. In terms of the first class, dark channel prior (DCP) method is a representative example, initially proposed by He *et al.* [11]. More recently, most methods using single image have been inspired by DCP that was employed to dehaze images taken in the atmosphere. For instance, a general boundary constraint strategy for generating a better transmission is introduced by Meng *et al.* [12]. Drews *et al.* [13] proposed the underwater DCP (UDCP) method for estimating the transmission of underwater scenes. All these methods focused on the estimation of transmission as accurate as possible only from single input image, which is a very challenging problem. For the second class, polarization-based image dehazing method is the most fashionable one, and it used two or more images captured in different directions of polarization to estimate the scene depth information by exploring the polarization property of scattered light. For instance, Schechner *et al.* [9] developed a polarization-difference imaging method to restore the quality of the degraded image and obtained positive results. Further research work has been proposed to extend this method in recent years [14]–[17], which proves that the polarimetric method is effective in improving the image quality.

Although these polarization-based image dehazing methods have several advantages, such as low computational cost and high efficiency, it often requires a precise selection of an image region where the target does not appear (called background region or sky region) for estimation of the key parameters,

Manuscript received June 19, 2020; revised July 28, 2020; accepted August 31, 2020. This work was supported in part by the National Natural Science Foundation of China under Grant 61802043 and Grant 62002043, in part by the Liaoning Revitalization Talents Program under Grant XLYC1908007, in part by the Foundation of Liaoning Key Research and Development Program under Grant 201801728, in part by the Fundamental Research Funds for the Central Universities under Grant 3132016352 and Grant 3132020215, and in part by the Dalian Science and Technology Innovation Fund under Grant 2018J12GX037 and Grant 2019J11CY001. *(Corresponding authors: Yafei Wang; Xianping Fu.)*

Zheng Liang, Xueyan Ding, Zetian Mi, and Yafei Wang are with the School of Information Science and Technology, Dalian Maritime University, Dalian 116026, China (e-mail: zliang@dlmu.edu.cn; dingxueyan@dlmu.edu.cn; mizetian@dlmu.edu.cn; wangyafei@dlmu.edu.cn).

Xianping Fu is with the School of Information Science and Technology, Dalian Maritime University, Dalian 116026, China, and also with the Peng Cheng Laboratory, Shenzhen 518000, China (e-mail: fxp@dlmu.edu.cn).

Color versions of one or more of the figures in this letter are available online at http://ieeexplore.ieee.org.

Digital Object Identifier 10.1109/LGRS.2020.3023805

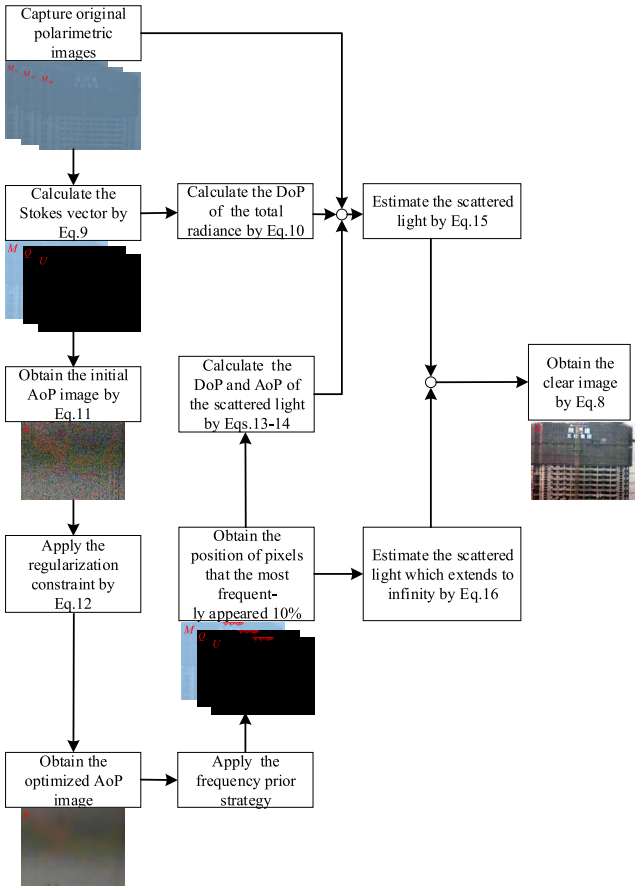

Fig. 2. Overview of the proposed method.

which is difficult to apply in the real world. In addition, photon noise, a well-known fundamental quantum-mechanical effect, cannot be overcome regardless of the quality of the camera. However, most of the existing polarization-based image dehazing techniques ignore this fact, resulting in terrible noise in the dehazed images.

In this letter, we propose an effective polarimetric image dehazing method based on the polarization difference that the scattered light is partially polarized and the reflected object light is unpolarized. Fig. 2 shows the overview of the proposed method. The proposed method robustly improves the visibility quality of the degraded images. We summary the specific contributions as follows.

1) An effective polarization-based image dehazing method by exploring the relationship between the angle of polarization (AoP) from the Stokes vector and the scattered light is proposed. The extensive validation reveals that the restored images of our method are characterized by better colors, improved global contrast, and lower noise.
2) A regularization constraint strategy is proposed to revise the information of AoP based on an assumption that adjacent pixels with similar colors have similar values of AoP.
3) An automatic and effective method is presented to estimate the key parameters without considering that the no-object region exists or not, which relies on a frequency prior strategy.

II. Proposed Methodology

A. Polarization-Based Dehazing Model

Schechner *et al.* [9] introduced a widely used polarization-based dehazing model in 2003, which can be given by

$$\begin{aligned} M^{\lambda}(i,j) &= D^{\lambda}(i,j) + A^{\lambda}(i,j) \\ &= N^{\lambda}(i,j)T^{\lambda}(i,j) + A^{\lambda}_{\infty}(1 - T^{\lambda}(i,j)) \end{aligned} \tag{1}$$

where M^{λ} denotes the image irradiance received by the camera and D^{λ} and A^{λ} indicate the reflect object irradiance and the scattered light irradiance, respectively. N^{λ} is the object radiance without any attenuation, T^{λ} represents the medium transmittance. A^{λ}_{∞} denotes the scattered light which extends to infinity, (i, j) is the pixel coordinate, and $\lambda = (r, g, b)$. Based on this model, two polarimetric images at orthogonal states ($M^{\lambda}_{\parallel}$ and $M^{\lambda}_{\perp}$, respectively) are acquired through rotating the polarizer mounted in front of the camera. They can be expressed as

$$M^{\lambda}_{\parallel}(i,j) = \frac{D^{\lambda}(i,j)}{2} + A^{\lambda}_{\parallel}(i,j) \tag{2}$$

$$M^{\lambda}_{\perp}(i,j) = \frac{D^{\lambda}(i,j)}{2} + A^{\lambda}_{\perp}(i,j). \tag{3}$$

Then, the total image irradiance can be written as

$$M^{\lambda}(i,j) = M^{\lambda}_{\parallel}(i,j) + M^{\lambda}_{\perp}(i,j). \tag{4}$$

In the polaization-based dehazing method, two crucial parameters are the degree of polarization (DoP) of scattered light p^{λ}_{A} and the scattered light, which extends to infinity A^{λ}_{∞}. To estimate the two parameters, most of polarization-based dehazing methods often manually marked a region where there exists no object as background region (or sky region), and they can be obtained by

$$p^{\lambda}_{A} = \frac{1}{|\Theta|} \sum_{(i,j)\in\Theta} \frac{M^{\lambda}_{\parallel}(i,j) - M^{\lambda}_{\perp}(i,j)}{M^{\lambda}_{\parallel}(i,j) + M^{\lambda}_{\perp}(i,j)} \tag{5}$$

$$A^{\lambda}_{\infty} = \frac{1}{|\Theta|} \sum_{(i,j)\in\Theta} \left[M^{\lambda}_{\parallel}(i,j) + M^{\lambda}_{\perp}(i,j)\right] \tag{6}$$

where Θ indicates the no-object region (or sky region) in the image. $|\Theta|$ denotes the total number of pixels in the region. Then, the scattered light can be estimated by

$$A^{\lambda}(i,j) = \frac{M^{\lambda}_{\parallel}(i,j) - M^{\lambda}_{\perp}(i,j)}{p^{\lambda}_{A}} \tag{7}$$

and according to (1), the haze-free image can be addressed by

$$N^{\lambda}(i,j) = \frac{M^{\lambda}(i,j) - A^{\lambda}(i,j)}{1 - \left[A^{\lambda}(i,j)/A^{\lambda}_{\infty}\right]}. \tag{8}$$

B. Estimation of Parameters A^{λ}_{∞} and p^{λ}_{A}

In the proposed method, a rotating linear polarizer is put in front of the camera, and through rotating the angle of polarizer to 0°, 45°, and 90°, three original polarimetric images $M^{\lambda}_{0}(i,j)$, $M^{\lambda}_{45}(i,j)$, and $M^{\lambda}_{90}(i,j)$ can be obtained, respectively. The Stokes vector can be written as

$$\begin{aligned} M^{\lambda}(i,j) &= M^{\lambda}_{0}(i,j) + M^{\lambda}_{90}(i,j) \\ Q^{\lambda}(i,j) &= M^{\lambda}_{0}(i,j) - M^{\lambda}_{90}(i,j) \\ U^{\lambda}(i,j) &= 2M^{\lambda}_{45}(i,j) - M^{\lambda}(i,j) \end{aligned} \tag{9}$$

where M^λ represents the total intensity of light detected by the camera and Q^λ and U^λ represent the intensity information of the linear polarization state. According to the polarization difference that the scattered light is partially polarized and the reflected object light is unpolarized, Q^λ and U^λ are mainly caused by the scattered light. From (9), the DoP of the total radiance $p^\lambda(i,j)$ and the AoP of the total radiance $\theta^\lambda(i,j)$ can be obtained by

$$p^\lambda(i,j) = \frac{\sqrt{\left[Q^\lambda(i,j)\right]^2 + \left[U^\lambda(i,j)\right]^2}}{M^\lambda(i,j)} \tag{10}$$

$$\theta^\lambda(i,j) = \frac{1}{2}\arctan\left[\frac{U^\lambda(i,j)}{Q^\lambda(i,j)}\right]. \tag{11}$$

According to (11), all the values of θ^λ are almost contributed by the scattered light, which provides a helpful support for estimating the two key parameters p_A^λ and A_∞^λ. Since the estimation of parameters is directly related to the information of AoP, to avoid the impact of quantization noise caused by camera itself, we design a regularization constraint strategy to optimize the information of θ^λ, which is based on an assumption that adjacent pixels with similar colors have similar values of AoP. This assumption is reasonable because scattered light is uniformly superimposed on a small image patch. Mathematically, the optimization function is defined by

$$E\left(\theta^\lambda\right) = \sum_{(i,j)}\sum_{(x,y)\in N(i,j)} \frac{\left[\theta^\lambda(i,j) - \theta^\lambda(x,y)\right]^2}{\|M^\lambda(i,j) - M^\lambda(x,y)\|_2^2} + \beta\sum_{(i,j)}\left[\theta^\lambda(i,j) - \tilde{\theta^\lambda}(i,j)\right]^2 \tag{12}$$

where $E(\theta^\lambda)$ is the energy function, and the final optimized AoP image θ^λ is computed by minimizing the function. $(x,y) \in N(i,j)$ denotes (x,y) that is adjacent to (i,j), $\tilde{\theta^\lambda}$ is the initial estimation of AoP, and β denotes a positive parameter in [0,1] that controls the degree of smoothness (0.05 in this letter).

After the optimized AoP image is obtained, an automatic and effective method is introduced to estimate the key parameters, which relies on a frequency prior strategy. In detail, first, we count the frequency of occurrence of each pixel value. Then, pixel values are sorted by frequency from high to low. Finally, we select the most frequently appeared 10% of pixel values as the values of AoP of the scattered light. Why not select all the values as the values of AoP of the scattered light? There are two reasons for it: on one hand, there might be a few other different values because the reflected light from the object closed to the camera might also have partial polarization properties; on the other hand, the original polarimetric images with three specific angles are obtained by manually rotating the polarizer, which is difficult to accurately obtain these raw images. As the position of these pixels is determined, the DoP and AoP of the scattered light are estimated by

$$p_A^\lambda = \frac{1}{|\Delta|}\sum_{(i,j)\in\Delta}\frac{\sqrt{\left(Q^\lambda(i,j)\right)^2 + \left(U^\lambda(i,j)\right)^2}}{M^\lambda(i,j)} \tag{13}$$

$$\theta_A^\lambda = \frac{1}{2|\Delta|}\sum_{(i,j)\in\Delta}\arctan\left[\frac{U^\lambda(i,j)}{Q^\lambda(i,j)}\right] \tag{14}$$

where Δ denotes the position of pixels that the most frequently appeared 10% in the AoP image θ^λ and $|\Delta|$ is the total number of pixels. With known p_A^λ and θ_A^λ, the scattered light A can be formulated according to the [15] as

$$A^\lambda(i,j) = \frac{M_0^\lambda(i,j) - M^\lambda(i,j)\left[1 - p^\lambda(i,j)\right]/2}{p_A^\lambda \cdot \cos^2\theta_A^\lambda}. \tag{15}$$

In addition, inspired by He *et al.* [11], among these pixels selected using the frequency prior technique, the scattered light that extends to infinity A_∞^λ can be estimated by minimizing the distance from the pure white vector $(255,255,255)$

$$\begin{aligned} A_\infty^\lambda &= M^\lambda\left(i^*, j^*\right) \text{ with} \\ \left(i^*, j^*\right) &= \underset{(i,j)|(i,j)\in\Delta}{\arg\min} \left\|\left(M^r(i,j), M^g(i,j), M^b(i,j)\right) - (255,255,255)\right\| \end{aligned} \tag{16}$$

where (i^*, j^*) denotes the location of the brightest pixel in the total intensity image M^λ. As the parameters A^λ and A_∞^λ are estimated, the haze-free image can be easily obtained using (8).

III. Experiments and Discussion

To verify the performance of the proposed method, several real-world polarimetric image dehazing samples are conducted. The experiments are grouped into two classes: comparison results based on images taken in atmosphere and comparison results based on images captured under water. In our experiments, an 8-bit digital COMS camera (Nikon D5300) with a linear polarizer is used to capture the raw polarimetric images under natural illumination. Three raw polarimetric images with specific angles (0°, 45°, and 90°) are captured through rotating the polarizer to different orientations.

A. Qualitative Results

First, an ablation study is proposed to demonstrate the effectiveness of the proposed method. Fig. 1 shows an example about visual comparisons. Fig. 1(a)–(c) shows three raw polarimetric images, Fig. 1(d) shows the total intensity image, Fig. 1(e) and (f) shows the initial AoP and optimized AoP image, respectively, and Fig. 1(g) and (h) shows the dehazed results generated using the initial AoP image and the optimized AoP image, respectively. It can be observed that the proposed method provides a satisfactory dehazed result with natural appearance, lower noise, and sufficient details.

Then, the classical Schechner and Karpel's method [18], DCP method [11], and Zhu *et al.*'s method [19] are used as the reference methods for assessing the effectiveness of the proposed method. Fig. 3 shows the visual results of different methods on three remotely sensed images. These raw images are captured under different densities of haze and the total intensity image from the Stokes vector is used as the input image in the DCP method and Zhu *et al.*'s method [19]. As we can see in Fig. 3, the details of the total intensity images

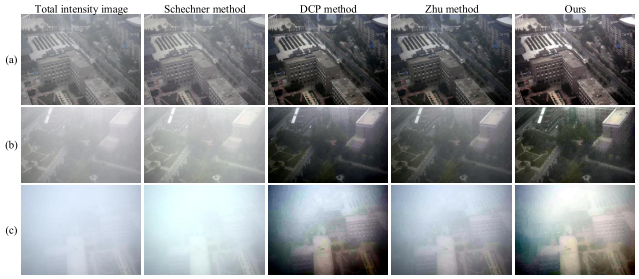

Fig. 3. Comparison of dehazed results generated using different methods on remotely sensed images. (a)–(c) are images taken under the atmosphere environment with different hazes. From the second column to the last column: Schechner and Karpel's method [18], DCP method [11], Zhu *et al.*'s method [19], and ours.

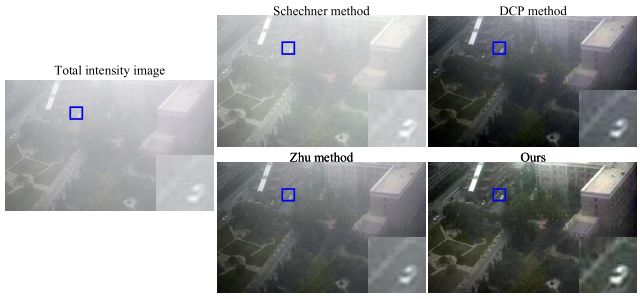

Fig. 4. Comparison of dehazed results generated using different methods on the distant region. Compared with other techniques, the car located on the distant region can be effectively dehazed by our method.

are severely degraded. Among these comparative methods, the Schechner method relies too much on the presence of the sky region when estimating the key prameters. However, it is difficult to find such region in these images and the results of their method do not perform well. DCP method and Zhu *et al.*'s method [19] can improve the overall quality. However, the dehazed images generated by their methods still suffer from lots of haze. In contrast, the proposed method yields results with fine details and vivid color and performs much better than other methods. As shown in Fig. 4, the proposed technique can efficiently remove haze from the near as well as the distant regions.

In addition, to evaluate the proposed method in a full-reference way, we also try to restore the degraded underwater images and compare the restored images with the ground-truth images. The comparison results are presented in Fig. 5. Meanwhile, the ground-truth images (taken in clear water) are also presented. As we can see in these examples, the results generated by the Schechner method suffer from the worst performance among these methods, which may be related to our failure to correctly select the background region. The results of DCP method often look darker and also suffer from severe color distortion. Zhu *et al.*'s method [19] shows a limitation in terms of removing haze. The proposed method provides more satisfactory results both in color and detail among these comparative validations, which is more similar to the ground-truth images.

B. Quantitative Results

In terms of Fig. 3, we perform the quantitative comparison based on the blind measure used in [20] and [21] and the entropy measure. In addition, the no-reference perceptual haze

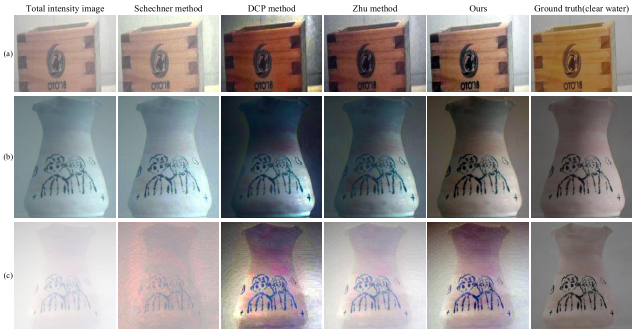

Fig. 5. Comparison of dehazed results generated using different methods on underwater images. (a)–(c) are images in turbid water with different densities of milk. From the second column to the last column: Schechner and Karpel's method [18], DCP method [11], Zhu *et al.*'s method [19], ours, and the ground truth.

TABLE I
QUANTITATIVE EVALUATION OF FIG. 3

Images	Metrics	Schechner	DCP	Zhu	Ours
Fig.3(a)	$E \uparrow$	6.9466	7.3044	7.2427	**7.6244**
	$\sigma \downarrow$	**0**	2.5494	0.2182	0.8080
	$\bar{r} \uparrow$	1.1543	1.5352	1.3443	**2.0900**
	$D \downarrow$	0.9690	0.3007	0.4376	**0.2845**
Fig.3(b)	$E \uparrow$	6.7102	**7.4356**	7.2975	7.0138
	$\sigma \downarrow$	0	1.9570	0	**0**
	$\bar{r} \uparrow$	1.4667	2.0235	1.8321	**3.7190**
	$D \downarrow$	3.7400	0.8578	1.5993	**0.6683**
Fig.3(c)	$E \uparrow$	6.0705	7.8178	7.1152	**7.8835**
	$\sigma \downarrow$	0	3.0140	0	**0**
	$\bar{r} \uparrow$	1.0752	2.8902	1.8476	**4.0115**
	$D \downarrow$	7.0893	**1.7871**	4.7689	2.1445

density assessment metric [20] is also used to assess the dehazing performance of the proposed method. The quantitative results are listed in Table I. The indicators $\bar{r}$ and σ denote the quality of the contrast restoration and the percentage of saturated pixels in the dehazed images, respectively. The indicators E and D are the values of the entropy and haze density, respectively. The values in bold indicate the best results. According to Table I, the proposed method can improve the contrast and details. Although the proposed method is slightly lower than other methods in terms of the entropy value of Fig. 3(b), the result of the proposed method is clearer.

Because the ground-truth images are available in these examples as shown in Fig. 5, two full-reference image restoration quality evaluation metrics (structural SIMilarity (SSIM) [22] and patch-based contrast quality index (PCQI) [23]) are used for quantitative assessment. The SSIM metric is a measurement of SSIM between the restored image and the ground-truth image. PCQI is introduced to quantitatively evaluate the performance in image contrast enhancement. The evaluation scores of three samples are presented in Table II, and the values in bold indicate the best results. It can be found that the proposed method performs the best on most metrics.

Overall, we conclude that the proposed method generally results in better appearance, with sufficient restoration of the color and the structure.

TABLE II
QUANTITATIVE SSIM AND PCQI VALUES OF FIG. 5

Assessments	Methods	Fig.5(a)	Fig.5(b)	Fig.5(c)
SSIM↑	Schechner	0.6108	0.0275	0.5299
	DCP	0.6598	0.0987	0.4939
	Zhu	0.6317	0.2006	**0.6684**
	Ours	**0.6880**	**0.7637**	0.6194
PCQI↑	Schechner	0.5278	0.6231	0.4397
	DCP	0.5615	0.6964	0.5458
	Zhu	0.5957	0.7515	0.4766
	Ours	**0.6482**	**0.8052**	**0.5652**

TABLE III
COMPUTATIONAL COST OF COMPARATIVE METHODS

Assessments	Schechner	DCP	Zhu	Ours
Run time(sec)	0.1265	45.5034	4.5624	5.4731

C. Computational Cost

Since our method conducts in a pixelwise manner and the action employed on each pixel with the complexity $O(1)$, the computational complexity of our technique is $O(mn)$ with a given image with the size of $m \times n$. We also compare the proposed method with other competitive methods in terms of the time cost. Table III reports the mean values. The execution time test was done on a 64-bit PC with Intel Core i3 CPU at 3.2 GHz and 8-GB RAM. The size of all the sample images is 640×480. It should be noted that the manual selection process of the background region is not included in the execution time of the Schechner method. As observed in Table III, the computational efficiency of the proposed method is not perfect, which still needs to be further improved in our future works.

IV. CONCLUSION

In this letter, a polarimetric image dehazing method by exploring the relationship between the information of AoP and the scattered light is proposed. Based on a reasonable assumption that the adjacent pixels with similar colors have similar values of AoP, the AoP image is optimized by minimizing the optimization function. Then, according to the optimized AoP image, we design a strategy to automatically obtain the key parameters in the proposed method without considering the no-object region (or the sky region) exists or not, which further improves the practical applicability of the proposed method. The extensive validation reveals that the restored images of our method are characterized by better colors, improved global contrast, and lower noise.

REFERENCES

[1] B. A. Levedahl and L. Silverberg, "Control of underwater vehicles in full unsteady flow," *IEEE J. Ocean. Eng.*, vol. 34, no. 4, pp. 656–668, Oct. 2009.

[2] C. Mazel, "*in situ* measurement of reflectance and fluorescence spectra to support hyperspectral remote sensing and marine biology research," in *Proc. OCEANS*, Sep. 2006, pp. 1–4.

[3] N. Strachan, "Recognition of fish species by colour and shape," *Image Vis. Comput.*, vol. 11, no. 1, pp. 2–10, Jan. 1993.

[4] Q. Zhang, H. Wang, J. Dong, G. Zhong, and X. Sun, "Prediction of sea surface temperature using long short-term memory," *IEEE Geosci. Remote Sens. Lett.*, vol. 14, no. 10, pp. 1745–1749, Oct. 2017.

[5] J. Long, Z. Shi, W. Tang, and C. Zhang, "Single remote sensing image dehazing," *IEEE Geosci. Remote Sens. Lett.*, vol. 11, no. 1, pp. 59–63, Jan. 2014.

[6] J. Li, Q. Hu, and M. Ai, "Haze and thin cloud removal via sphere model improved dark channel prior," *IEEE Geosci. Remote Sens. Lett.*, vol. 16, no. 3, pp. 472–476, Mar. 2019.

[7] M. Ju, C. Ding, D. Zhang, and Y. J. Guo, "Gamma-Correction-Based visibility restoration for single hazy images," *IEEE Signal Process. Lett.*, vol. 25, no. 7, pp. 1084–1088, Jul. 2018.

[8] T. Liu *et al.*, "Polarimetric underwater image recovery for color image with crosstalk compensation," *Opt. Lasers Eng.*, vol. 124, Jan. 2020, Art. no. 105833.

[9] Y. Y. Schechner, S. G. Narasimhan, and S. K. Nayar, "Polarization-based vision through haze," *Appl. Opt.*, vol. 42, no. 3, pp. 511–525, Jan. 2003.

[10] C. Ancuti and C. O. Ancuti, "Effective contrast-based dehazing for robust image matching," *IEEE Geosci. Remote Sens. Lett.*, vol. 11, no. 11, pp. 1871–1875, Nov. 2014.

[11] K. He, J. Sun, and X. Tang, "Single image haze removal using dark channel prior," *IEEE Trans. Pattern Anal. Mach. Intell.*, vol. 33, no. 12, pp. 2341–2353, Dec. 2011.

[12] G. Meng, Y. Wang, J. Duan, S. Xiang, and C. Pan, "Efficient image dehazing with boundary constraint and contextual regularization," in *Proc. IEEE Int. Conf. Comput. Vis.*, Dec. 2013, pp. 617–624.

[13] P. Drews, Jr., E. do Nascimento, F. Moraes, S. Botelho, and M. Campos, "Transmission estimation in underwater single images," in *Proc. IEEE Int. Conf. Comput. Vis. Workshops*, Dec. 2013, pp. 825–830.

[14] H. Tian *et al.*, "Rapid underwater target enhancement method based on polarimetric imaging," *Opt. Laser Technol.*, vol. 108, pp. 515–520, Dec. 2018.

[15] W. Zhang, J. Liang, L. Ren, H. Ju, Z. Bai, and Z. Wu, "Fast polarimetric dehazing method for visibility enhancement in HSI colour space," *J. Opt.*, vol. 19, no. 9, Sep. 2017, Art. no. 095606.

[16] H. Hu *et al.*, "Polarimetric image recovery in turbid media employing circularly polarized light," *Opt. Express*, vol. 26, no. 19, pp. 25047–25059, 2018.

[17] J. Liang, W. Zhang, L. Ren, H. Ju, and E. Qu, "Polarimetric dehazing method for visibility improvement based on visible and infrared image fusion," *Appl. Opt.*, vol. 55, no. 29, pp. 8221–8226, 2016.

[18] Y. Y. Schechner and N. Karpel, "Clear underwater vision," in *Proc. IEEE Comput. Soc. Conf. Comput. Vis. Pattern Recognit.*, 1998, p. 1.

[19] Q. Zhu, J. Mai, and L. Shao, "A fast single image haze removal algorithm using color attenuation prior," *IEEE Trans. Image Process.*, vol. 24, no. 11, pp. 3522–3533, Nov. 2015.

[20] D. Singh, V. Kumar, and M. Kaur, "Image dehazing using window-based integrated means filter," *Multimedia Tools Appl.*, vol. 12, pp. 1–23, Nov. 2019.

[21] M. Kaur, D. Singh, V. Kumar, and K. Sun, "Color image dehazing using gradient channel prior and guided l0 filter," *Inf. Sci.*, vol. 521, pp. 326–342, Jun. 2020.

[22] C. Li, S. Anwar, and F. Porikli, "Underwater scene prior inspired deep underwater image and video enhancement," *Pattern Recognit.*, vol. 98, Feb. 2020, Art. no. 107038.

[23] S. Wang, K. Ma, H. Yeganeh, Z. Wang, and W. Lin, "A patch-structure representation method for quality assessment of contrast changed images," *IEEE Signal Process. Lett.*, vol. 22, no. 12, pp. 2387–2390, Dec. 2015.